The Chain-Link Actuator: Exploiting the Bending Stiffness of McKibben Artificial Muscles to Achieve Larger Contraction Ratios

Daniel Bruder [ORCID], *Member, IEEE*, and Robert J. Wood

Abstract—McKibben artificial muscles, comprised of an expandable bladder wrapped in a double-helix-braided sheath, have the ability to generate forces without restricting motion to occur exclusively along the direction of actuation. This makes them attractive for a variety of applications including soft, wearable, and biomimetic robots. Despite their advantages, the theoretical maximum contraction ratio of McKibben muscles is only 36.3%, which restricts the range of motion of the systems they actuate. This work introduces a novel 'chain-link actuator' that exploits the bending stiffness of McKibben muscles to achieve contraction ratios of more than 50%. A static model that captures the relationship between pressure, displacement, and force is presented and validated on several real chain-link actuator systems.

Index Terms—Pneumatic actuator, soft robotics.

I. INTRODUCTION

THE McKibben artificial muscle (sometimes referred to as the Pneumatic Artificial Muscle or PAM) was developed in the 1950 s and 1960 s with the intended purpose of actuating orthotic devices and artificial limbs [1]. McKibben muscles contract upon pressurization,[1] mimicking the force-displacement relationship exhibited by biological muscles. Comprised of just an expandable bladder wrapped in a double-helix-braided sheath, McKibben muscles are easy to fabricate, lightweight, and compliant, yet capable of generating large forces when fully extended [2]. For this reason, they have been widely used in many biorobotic, medical, industrial, and aerospace applications over the years [3], including walking robots [4]–[7], arms [8], [9], orthotic devices [10]–[15], and morphing wings [16].

Despite their wide use, McKibben muscles suffer from a limited contraction ratio, which restricts the range of motion of McKibben actuated systems such as soft robots [17], wearable robots [18], and biomimetic robots [19]. The theoretical maximum contraction ratio for a McKibben muscle is $\approx 36.3\%$, but

[1]McKibben muscles can also be made that expand upon pressurization, but we limit our discussion to the contractile type in this letter.
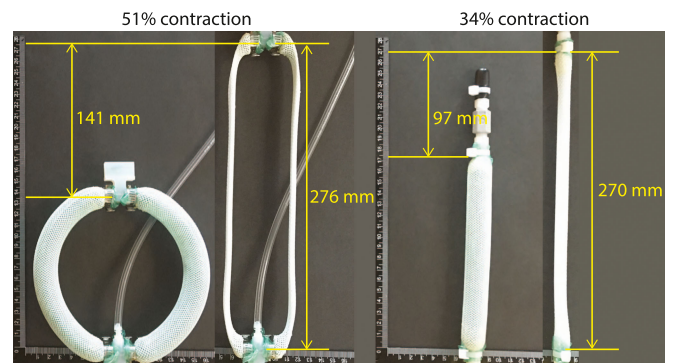

Fig. 1. The chain-link actuator (left) consists of two McKibben artificial muscles with their ends mounted perpendicular to the axis of contraction. When pressurized to 200 kPa, the chain-link actuator contracts by 51% of its maximum length, whereas a McKibben in its standard orientation (right) only contracts by 34% of its maximum length.

in practice only 20-30% is typically achieved due to friction, bladder stiffness, edge effects, and other non-idealized phenomena [20].

In this paper, we show how this contraction limit can be overcome by exploiting an often overlooked characteristic of McKibben muscles: their bending stiffness. McKibben muscles are prized for their ability to generate forces without restricting motion to occur exclusively along the primary direction of actuation, yet they still contribute forces in off-axis directions. As this paper will demonstrate, a pressurized McKibben actuator actually behaves much like an elastic rod with a preference for being straight.

We orient the ends of the McKibben muscle perpendicular to the direction of contraction rather than parallel to it (see Fig. 1), and mount a second McKibben opposite the first. This arrangement of two McKibbens forms a contractile actuator module which we refer to as a *chain-link actuator*. For a given displacement, the McKibbens take on the shape that minimizes the strain energy stored in their outer walls, resulting in a curved shape that traces a longer path between endpoints than a straight line. To achieve maximum volume in this configuration, the McKibbens must bring their ends closer together than when their ends are parallel to the axis of contraction, thus achieving a larger contraction ratio than a traditional McKibben configuration. In several experiments, we observe the chain-link actuator exhibiting contraction ratios greater than 50%.
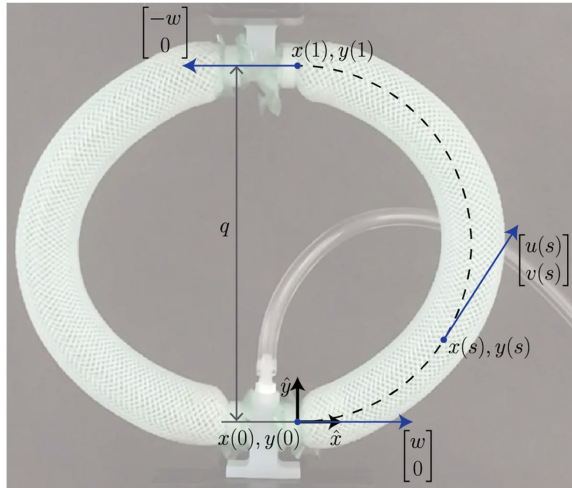
Fig. 2. The shape of one side of a chain-link actuator is parameterized by the polynomial functions $x(s), y(s)$ and the velocity along the curve is described by the vector $[u(s), v(s)]$.

This work is not the first to propose a geometrical arrangement of McKibbens that overcomes the contraction ratio of a McKibben in the standard orientation. Actuators comprised of several McKibben actuators braided together in [21], [22] achieved contraction ratios of up to 41%. However, one downside of this arrangement is that the friction between McKibben actuators after braiding increases hysteresis. While in some applications hysteresis can be useful, it introduces nontrivial modeling and control challenges. The chain-link actuator exhibits relatively little hysteresis by comparison.

We present herein a chain-link actuator model that is linear with respect to pressure, enabling efficient computation of the pressure needed to achieve a desired displacement. We validate this model against force measurements from a real chain-link actuator, and we demonstrate how this model can be used to predict the relationship between the pressure and displacement of a chain of 4 chain-link actuators connected in series.

The rest of this paper is organized as follows: Section II describes the proposed actuator model. Section III describes several model validation experiments and their results. Section IV discusses the results of the experiments and concludes the paper.

II. MODELING

This section describes the modeling framework for the proposed actuator. As shown in Fig. 1, the chain-link actuator is composed of two identical McKibben actuators mounted opposite one another, perpendicular to the direction of contraction. The symmetry of this arrangement allows us to model the total force output by simply doubling the contribution of just one of the McKibben actuators. Therefore, the modeling framework that follows characterizes the behavior of just a single McKibben with ends oriented as shown in Fig. 2.

The proposed model describes the force generated by the chain-link actuator in terms of its geometry and internal pressure without any dependence on empirically derived material parameters such as elasticity or Young's modulus. It is premised

on the assumption that the fibers in a McKibben muscle are inextensible and thus incapable of storing strain energy.

The law of conservation of energy dictates that the fluid energy into a McKibben muscle must equal the sum of mechanical energy out, potential energy storage, and heat loss. With inextensible fibers we assume there is negligible energy storage, and we additionally assume negligible heat loss. Therefore, in our model the fluid power P_{fluid} is perfectly transformed into mechanical power P_{mech}, i.e.

$$P_{\text{mech}} = P_{\text{fluid}} \Rightarrow \frac{dq}{dt}\tau = \frac{dV}{dt}p \qquad (1)$$

where q is the actuator displacement, p is the internal pressure, V is the enclosed fluid volume, and τ is the force generated along the direction of the displacement variable q.

The fibers impose a kinematic constraint on the enclosed volume such that it can be expressed as a function of the actuator displacement q. Therefore, by the chain rule,

$$\frac{dV}{dt} = \frac{\partial V}{\partial q}\frac{dq}{dt} = J_q(q)\frac{dq}{dt} \qquad (2)$$

Here, we replace $\frac{\partial V}{\partial q}$ with the notation J_q and refer to it as the *fluid Jacobian*. Substituting (2) into (1) and simplifying then yields the following expression for force in terms of the actuator displacement and pressure,

$$\tau(q, p) = J_q(q)p \qquad (3)$$

Formulating McKibben actuator force in terms of a fluid Jacobian was first introduced in [23], and is consistent with the virtual work formulation found in [24] and elsewhere.

The remainder of this section describes the derivation the fluid Jacobian for the chain-link actuator. Section II-A describes a parameterization of the shape of the actuator. Section II-B describes the force due to the work done by the fluid. Section II-C describes the method used to identify the best value of a key shape parameter. Section II-D describes how each of the preceding components are combined into a single equation.

A. Shape Parameterization

We approximate the shape of the McKibben as a third degree polynomial function of the parameterization variable $s \in [0, 1]$.

$$x(s) = \alpha_0 + \alpha_1 s + \alpha_2 s^2 + \alpha_3 s^3 \qquad (4)$$

$$y(s) = \beta_0 + \beta_1 s + \beta_2 s^2 + \beta_3 s^3 \qquad (5)$$

where $\alpha_0, \ldots, \alpha_3$ and $\beta_0, \ldots, \beta_3$ are constant coefficients.

The shape parameterization must satisfy the following boundary conditions,

$$x(0) = \alpha_0 = 0 \qquad (6)$$

$$y(0) = \beta_0 = 0 \qquad (7)$$

$$x(1) = \alpha_0 + \alpha_1 + \alpha_2 + \alpha_3 = 0 \qquad (8)$$

$$y(1) = \beta_0 + \beta_1 + \beta_2 + \beta_3 = q \qquad (9)$$

$$\left.\frac{dx}{ds}\right|_{s=0} = \alpha_1 = \omega \qquad (10)$$

$$\left.\frac{dy}{ds}\right|_{s=0} = \beta_1 = 0 \tag{11}$$

$$\left.\frac{dx}{ds}\right|_{s=1} = \alpha_1 + 2\alpha_2 + 3\alpha_3 = -\omega \tag{12}$$

$$\left.\frac{dy}{ds}\right|_{s=1} = \beta_1 + 2\beta_2 + 3\beta_3 = 0 \tag{13}$$

for some positive constant ω which we refer to as the "shape speed" because it describes the speed of a particle traveling along the shape curve at the endpoints. (6)–(9) ensure the curve has the correct endpoints while equations (10)–(13) ensure that the shape curve is horizontal at $s = 0, 1$.

Simultaneously solving (6)–(13) yields the following parametrization in terms of the actuator displacement q and the "shape speed" ω,

$$x(s) = \omega s - \omega s^2 \tag{14}$$

$$y(s) = 3qs^2 - 2qs^3 \tag{15}$$

For convenience we introduce the notation u, v to represent the derivative functions of x and y with respect to s,

$$u(s) = \frac{dx(s)}{ds} = \omega - 2\omega s \tag{16}$$

$$v(s) = \frac{dy(s)}{ds} = 6qs - 6qs^2 \tag{17}$$

The shape speed parameter ω is chosen such that the resulting shape minimizes the total strain energy of the system. The process for selecting this value is described in Section II-C.

B. Volume as a Function of Displacement

A fluid Jacobian requires an expression of volume as a function of the displacement variable. We model the geometry of each McKibben in a chain-link actuator as an extruded circle along the polynomial shape curve described in the previous section. We assume a constant radius over its entire length, ignoring tapering at the ends. Under these assumptions, the volume is simply given by $V = \pi r^2 \ell$ where r is the radius of the extruded tube and ℓ is the arc length of the shape curve, both of which are functions of the displacement variable q.

To find the length of the shape curve in terms of q, we approximate the arc length integral,

$$\ell = \int_0^1 \sqrt{u(s)^2 + v(s)^2}ds \tag{18}$$

as the finite sum over N_s slices

$$\approx \sum_{k=0}^{N_s-1} \frac{1}{N_s} \sqrt{u\left(\frac{k}{N_s}\right)^2 + v\left(\frac{k}{N_s}\right)^2} \tag{19}$$

We merely approximate ℓ rather than evaluating the integral in (18) because finding an explicit solution is intractable.

With an approximation of the arc length ℓ known, the radius is given by the following expression

$$r(q) = \sqrt{\frac{B_f^2 - \ell(q)^2}{(2\pi N_f)^2}} \tag{20}$$

where B_f is the unwound length of one of the McKibben fibers, and N_f is the number of revolutions made by one of the fibers over the McKibben's length. This relationship arises from the Pythagorean theorem applied to an unwound fiber [23].

Substituting (19) and (20) into the expression for the volume of an extruded circle yields the following expression,

$$V(q) = \pi r^2 \ell = \pi \frac{B_f^2 - \ell(q)^2}{(2\pi N_f)^2} \ell(q) \tag{21}$$

where ℓ is left in its unexpanded form to conserve space.

C. Selection of Shape Speed Parameter

When pressurized, McKibben actuators demonstrate a resistance to bending. This bending stiffness influences the shape an actuator takes. We account for this bending stiffness in our model by considering a McKibben to be analogous to a thin-walled planar beam and choosing the value of the shape parameter ω such that strain energy in the beam is minimized. In other words, we assume that the McKibben will take on the shape that minimizes strain energy while satisfying (6)–(13). Therefore, we select ω such that it satisfies the following optimization problem,

$$\min_{\omega} \quad U(\omega)$$
$$\text{s.t.} \quad 0 < \omega \tag{22}$$

where U is total strain energy in the planar beam analog. Note that this is a nonlinear optimization problem, therefore a globally optimal solution may not always be found. The remainder of this section describes the derivation of an expression for the total strain energy U.

Considering strain energy as a way to explain shape may seem incompatible with the modeling assumptions made earlier, namely that the actuator acts as a fluid-to-mechanical power transformer with negligible energy storage. We assume strain energy to be negligible in the derivation of (3) because it is small in magnitude relative to the total fluid energy of the system. However, it does come into play when determining the shape because the geometry of the actuator is not fully constrained by just its endpoints. Rather than including this strain energy in our energy balance formulation directly, we choose to encode it into the geometrical relationship between volume and displacement. This allows us to take the actuator's bending stiffness into consideration while preserving the linearity of the mapping between force and pressure.

Strain is defined relative to some reference, so we define the beam's "zero strain length" to be the same as the length of the McKibben in its maximum volume configuration. This is the configuration the McKibben would achieve in the absence of external forces given a nonzero actuation pressure, assuming the internal bladder does not resist deformation. Such an assumption is valid for bladders that expand by unfurling rather than stretching. For elastomeric bladders that deform by stretching, it is more suitable to define strain relative to the bladder's unstretched configuration, but we don't consider such cases in this work.

If we take the derivative of volume with respect to length then set it equal to zero, we find that the length that maximizes the
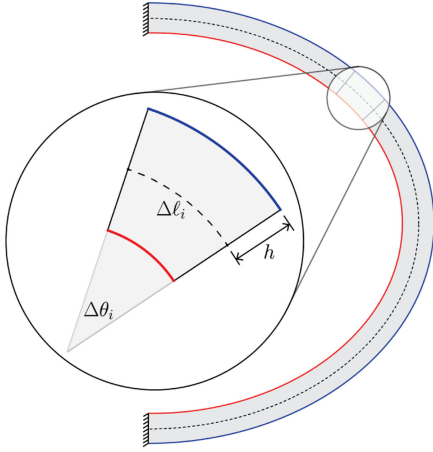
Fig. 3. A planar thin-walled beam of thickness $2h$ is used as an analog for a bent McKibben. Slices such as the one shown are assumed to have constant curvature. Curvature is exaggerated in the callout.

volume of a McKibben $\ell_{V_{\max}}$ is equal to the following,

$$\ell_{V_{\max}} = \frac{B_f}{\sqrt{3}} \qquad (23)$$

Then, the overall strain of the central axis ϵ_{axial} is defined relative to this nominal length as

$$\epsilon_{\text{axial}} = \frac{\ell - \ell_{V_{\max}}}{\ell_{V_{\max}}} \qquad (24)$$

To determine the strain density in the walls of the beam as a function of the shape parameterization variable s, we slice it along its axis into N_s slices and compute the strain density in each one. The slices are spaced equally along the length of the actuator with respect to the shape parameterization variable s, i.e. $\Delta s = \frac{1}{N_s}$. Note that this does not necessarily imply all slices will be of equal length. For N_s sufficiently large, each slice can be assumed to have constant curvature, as shown in Fig. 3.

The angle of curvature of the ith slice, $\Delta\theta_i$, is the angle between a vector tangent to the shape curve at $s_{i-1} = \frac{i-1}{N_s}$ and $s_i = \frac{i}{N_s}$. i.e.

$$\Delta\theta_i = \cos^{-1}\frac{z(s_i) \cdot z(s_{i-1})}{\|z(s_i)\| \, \|z(s_{i-1})\|} \qquad (25)$$

where $z(s_i) = [u(s_i), v(s_i)]^\top$. For sufficiently large N_s, the arc length of the central axis of the ith slice, $\Delta\ell_i$, is approximately

$$\Delta\ell_i \approx \Delta s\sqrt{u(s_i)^2 + v(s_i)^2} \qquad (26)$$

Assuming the strain at every point along the central axis is ϵ_{axial}, the nominal arc length of the central axis of the ith slice $\Delta\bar{\ell}_i$ would be

$$\Delta\bar{\ell}_i = \Delta\ell_i - \Delta\ell_i\epsilon_{\text{axial}} \qquad (27)$$

The strain in the beam wall can be expressed as a function of its distance from the central axis, denoted h in Fig. 3,

$$\epsilon(h) = \frac{(\Delta\ell_i + h\Delta\theta_i) - \Delta\bar{\ell}_i}{\Delta\bar{\ell}_i} = \epsilon_{\text{axial}} + \frac{h\Delta\theta_i}{\Delta\bar{\ell}_i} \qquad (28)$$

Therefore, for the ith slice, the strain in the inner wall $\epsilon_{\text{in},i}$ and outer wall $\epsilon_{\text{out},i}$ (shown in red and blue in Fig. 3, respectively) are given by the following expressions,

$$\epsilon_{\text{in},i} = \epsilon_{\text{axial}} - \frac{h\Delta\theta_i}{\Delta\bar{\ell}_i} \qquad (29)$$

$$\epsilon_{\text{out},i} = \epsilon_{\text{axial}} + \frac{h\Delta\theta_i}{\Delta\bar{\ell}_i} \qquad (30)$$

Since the walls of a thin-walled planar beam are one dimensional, its total strain energy U is found by integrating the strain density of the inner and outer walls over the length of the beam, i.e.

$$U = \int_0^1 \frac{1}{2}E\left(\epsilon_{\text{in}}(s)^2 + \epsilon_{\text{out}}(s)^2\right)ds \qquad (31)$$

where E is Young's Modulus, and $\epsilon_{\text{in/out}}(s)$ is a continuous strain density function for the inner and outer walls, respectively. For computational simplicity, we approximate this quantity by summing over the finite number of N_s slices

$$U \approx \sum_i^{N_s} \frac{1}{2}E\left(\epsilon_{\text{in},i}^2 + \epsilon_{\text{out},i}^2\right)\Delta\ell_i \qquad (32)$$

Note that when U is used as a cost function in (22) to select ω, the constants E and $\frac{1}{2}$ can be factored out. Thus, a Young's Modulus need not be assigned to the thin-walled beam analog.

D. Total Force

According to our model, the total force generated by a bent McKibben actuator is the product of its fluid Jacobian and internal pressure. The fluid Jacobian is computed by taking the derivative of the volume (21) with respect to displacement q,

$$J_q(q) = \frac{\partial V(q)}{\partial q} = \left(\frac{B_f^2 - 3\ell^2}{4\pi N_f^2}\right)\frac{\partial\ell}{\partial q} \qquad (33)$$

where $\frac{\partial\ell}{\partial q}$ is found by substituting (16) and (17) into (18) and taking the derivative with respect to q,

$$\frac{\partial\ell}{\partial q} = \int_0^1 \frac{72qs^2(1-s)^2}{\sqrt{\omega^2(1-2s)^2 + 36q^2\,s^2(1-s)^2}} \qquad (34)$$

Just as in (19), it is often more convenient to approximate this integral as a finite sum over N_s slices.

Since a chain-link actuator is comprised of two identical McKibbens muscles, the force must be multiplied by two. This yields the following formula for the net force generated by a chain-link actuator, τ_{cla}, with internal pressure p,

$$\tau_{\text{cla}}(q,p) = 2J_q(q)p \qquad (35)$$

III. MODEL VALIDATION EXPERIMENTS

A. Shape

We compared the polynomial shape parameterization described by (14) and (15) to the real shape of one of the McKibben muscles in a chain-link actuator with fiber length $B_f = 310$ mm and number of fiber revolutions $N_f = 3.5$ over the set of displacements $q =$
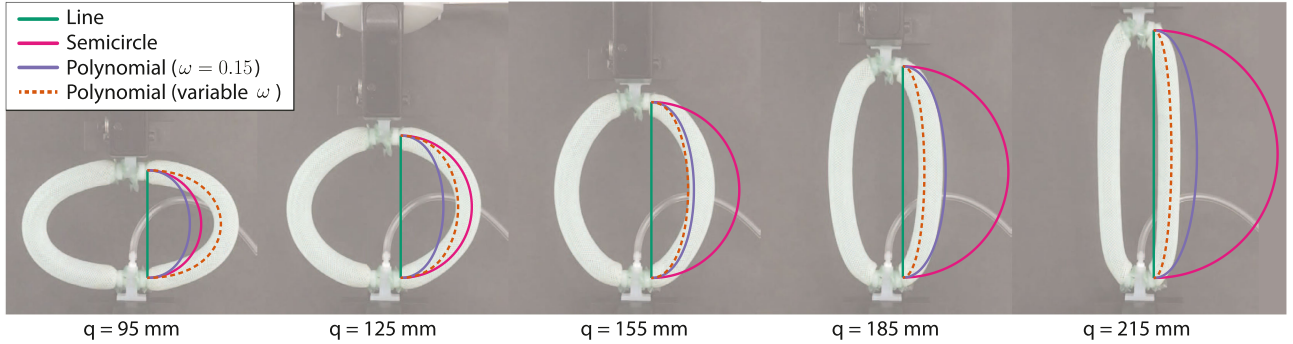
Fig. 4.   Various shape parameterizations superimposed on the actual shape of a chain-link actuator.

TABLE I
SHAPE PARAMETERIZATION ERROR (MIDPOINT TO MIDPOINT DISTANCE, MM)

q (mm)	95	125	155	185	215	Ave.
Line	68	58	43	23	11	41
Semicircle	21	5	34	69	96	45
Polynomial ($\omega = 0.15$)	31	20	6	14	26	19
Polynomial (ω = sol. to (22))	3	7	11	4	4	6

$\{95, 110, 125, 140, 155, 170, 185, 200, 215\}$ mm. For each displacement, the shape speed parameter ω was selected by solving (22), for a thin-walled planar beam analog with a width of $2h = 5$ mm.

The shape of the real actuator was also compared to several other shape parameterization types such as a straight line, semicircle, and polynomial with *fixed* speed parameter $\omega = 0.15$. A photograph was taken of the real chain-link actuator over several displacements. Fig. 4 shows each shape type superimposed onto the real McKibben. The coordinates of the midpoint of the McKibben were identified in each photo from pixel values. Then, the distance between these real midpoint coordinates and the midpont coordinates of each shape type was used as a simple quantitative measure of their accuracy. Table I provides a summary of these results, which show that our shape parameterizition is the most accurate and consistent across displacements.

B. Displacement Vs. Force (Pressure Fixed)

Our model's force predictions were validated using a 2 kN load cell mounted on an Instron tensile testing machine. Each McKibben actuator in the chain-link actuator had a fiber length $B_f = 310$ mm and number of fiber revolutions $N_f = 3.5$. Expandable sleeving with $1/2$ in ID made of polyester fabric was used for the fiber reinforcements (McMaster-Carr #9284K614), and the inner bladder was made of Stretchlon 200 bagging film (FibreGlast #1678).

Four trials were conducted for fixed internal pressures of $p = \{50, 100, 150, 200\}$ kPa. In each trial, the force was measured while q was smoothly varied from 215 mm to 95 mm, then back to 215 mm in order to capture any hysteric behavior. The

TABLE II
AVERAGE FORCE PREDICTION ERROR (N)

	Trial Pressure (kPa)			
	50	100	150	200
Trad. Model	26.5	53.8	80.5	105.7
Our Model	2.7	4.3	5.5	6.9

measured forces were compared to the force predictions of two models, which we refer to by the following names:

- *Traditional model:* Assumes straight line geometry between ends of McKibbens.
- *Our model:* Assumes shape as described in Section II-A.

Both models characterize force as the product of a fluid Jacobian and internal pressure. They differ only in the shape parameterization they use to derive the fluid Jacobian. The results are shown in Fig. 5 , and the prediction error of each model is provided in Table II .

C. Pressure Vs. Displacement (Force Fixed)

Our model can be be inverted to find the input pressure that achieves a desired displacement for a known force. Given a desired displacement q_{des} and known load force τ_{load}, we compute the corresponding fluid Jacobian J_q, plug it into (35), and solve for pressure p^*,

$$p^* = \frac{1}{2} J_q(q_{\text{des}})^{-1} \tau_{\text{load}} \qquad (36)$$

Our model's predictions for the relationship between displacement and pressure was evaluated using a chain of four chain-link actuators connected in series over three trials. The force was fixed in each trial by hanging a mass of 200 g, 500 g, and 1000 g to the end of the chain. Each of the McKibben actuators in the chain had a fiber length $B_f = 210$ mm and number of fiber rotations $N_f = 2.4$. Because the actuators were connected in series, the total displacement of the entire chain was simply the sum of the displacements of each chain-link actuator in the chain and the net force was equal to the force of each chain-link actuator.

For each load, we solved (36) for pressure given $q_{\text{des}} \in \{350, 351, \ldots, 700\}$mm, yielding a set of predicted displacement/pressure pairs. Then we evaluated those predictions on the real system by linearly varying the pressure from 0 kPa
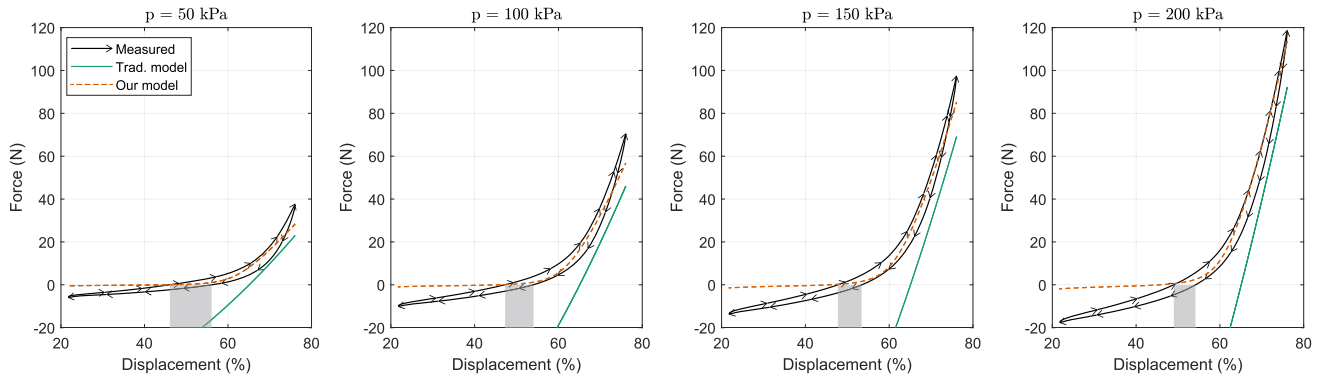
Fig. 5. Comparison of force vs. displacement predictions of the traditional McKibben model and our chain-link actuator model for fixed pressures of 50, 100, 150, and 200 kPa. The region between x-intercepts of the measured force curves during contraction and extension is shown in grey. Tensile forces are shown as positive.
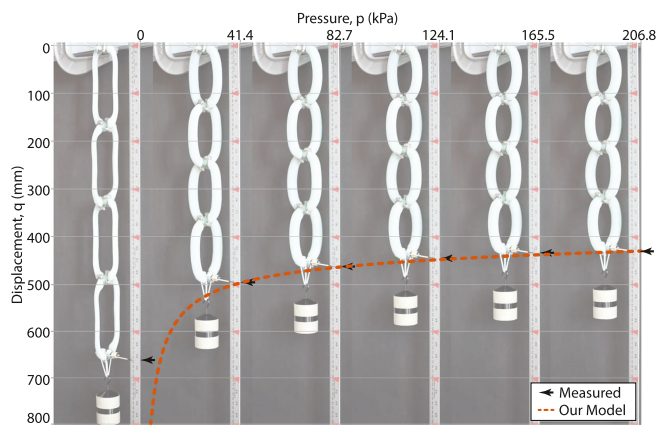

Fig. 6. Four chain-link actuators connected in series lift a 1 kg load as the pressure increases from 0 to 206.8 kPa. Model predictions computed by the process described in Section III-C (dashed orange line) are superimposed onto the real displacements (black arrows) at several pressures.

TABLE III
DISPLACEMENT ERROR FOR CHAIN-LINK ACTUATOR CHAIN

$\tau_{load}(N)$	Ave. Error (mm)
1.96	8.8
4.91	12.3
9.81	10.8

where $q_{des,j}$ is the desired displacement corresponding to p^* at time $3j$ seconds according to (36), and $q_{meas,j}$ is the measured displacement at that same pressure.

IV. DISCUSSION AND CONCLUSION

The results of our validation experiments confirm that the chain-link actuator is capable of larger displacements than a standard McKibben actuator and that our modeling approach is capable of predicting its force and displacement based on its geometry and pressure alone, without requiring the identification of material constants such as Young's Modulus.

As shown in Fig. 4, our proposed shape parameterization more accurately captures the observed geometry of a real chain-link actuator than several other shape types. Notably, fixing the shape speed parameter in the polynomial shape defined in (14) and (15) rather than identifying it via optimization yields a description that increasingly diverges from the true shape at the displacement extremes. This underscores the importance of selecting ω such that the resulting shape minimizes strain energy.

The force prediction comparison shown in Fig. 5 confirms the necessity of taking the bending stiffness of McKibben actuators into account. According to the traditional model, which assumes McKibbens have a straight line geometry between their end points, the predicted force is only accurate to within 66.6 N on average, which is 56% of the maximum measured force. Our model, which explicitly accounts for a McKibben's bent geometry and stiffness, is accurate to within 4.9 N on average, which is 4.1% of the maximum measured force. The largest deviation from the model predictions occurs in the regions where the force is negative. This suggests that the model is not sufficient for predicting compressive forces, despite its accuracy in predicting tensile forces. Future efforts could apply similar modeling approaches to McKibben actuated systems to better model their off-axis forces and predict their response in arbitrary configurations beyond the one explored in this paper.

The force measurements in Fig. 5 also confirm the capability of the chain-link actuator to achieve greater contraction ratios than a McKibben aligned with the axis of contraction. In all

to 200 kPa then back down to 0 kPa over 60 seconds. The displacement was measured manually from video footage every 3 seconds for a total of 21 measurements per trial.

Select snapshots of the 1000 g trail are shown in Fig. 6 for various pressures. The model predictions are superimposed on the measured displacement/pressure pairs, and Table III contains the average displacement error over all 21 measurements of each trial, defined as,

$$\frac{\sum_{j=0}^{20} |q_{des,j} - q_{meas,j}|}{21} \qquad (37)$$

four trials, the chain-link actuator's measured force output was equal to zero at displacements of 46-56% of its maximum length, indicating the displacement at which it achieves its maximum volume.

The model also proved capable of predicting the relationship between displacement and pressure given a known external force. As shown in Table III, the model proved capable of predicting the correct displacement to within 13 mm on average, which is roughly 4% of its total observed range of motion.

One potential downside of the chain-link actuator is its small stroke-to-width ratio when fully contracted. In applications where a low profile actuator is desired, the relatively large footprint of the chain-link actuator may be undesirable. However, as we have shown, the stroke-to-width ratio can be drastically increased by chaining several chain-link actuators together. Such an arrangement could be made as radially compact as a single McKibben relative to its stroke length given a long enough chain.

We have introduced a novel arrangement of McKibben actuators that exploits their bending stiffness to achieve contraction ratios of more than 50% and proposed a model that has been shown to make force and displacement predictions that are accurate to within 4.1% and 4% on average, respectively. With such a large contraction ratio and ability to accurately predict its force output, the chain-link actuator has the potential to become a popular choice for future wearable and soft robotics applications.

REFERENCES

[1] J. L. McKibben, "Artificial muscle," *Life*, vol. 10, no. 10, pp. 87–88, Mar. 1960.

[2] M. Mori, K. Suzumori, M. Takahashi, and T. Hosoya, "Very high force hydraulic mckibben artificial muscle with a p-phenylene-2, 6-benzobisoxazole cord sleeve," *Adv. Robot.*, vol. 24, no. 1/2, pp. 233–254, 2010.

[3] G. Andrikopoulos, G. Nikolakopoulos, and S. Manesis, "A survey on applications of pneumatic artificial muscles," in *Proc. 19th Mediterranean Conf. Control Automat.*, 2011, pp. 1439–1446.

[4] K. Berns, T. Kerscher, and J. Albiez, "Joint control of the six-legged robot AirBug driven by fluidic muscles," in *Proc. 3rd Int. Workshop Robot Motion Control*, 2002, pp. 27–32.

[5] H. Witte *et al.*, "Transfer of biological principles into the construction of quadruped walking machines," in *Proc. 2nd Int. Workshop Robot Motion Control (IEEE Cat. No 01EX535)*, 2001, pp. 245–249.

[6] R. Niiyama and Y. Kuniyoshi, "A pneumatic biped with an artificial musculoskeletal system," in *Proc. 4th Int. Symp. Adaptive Motion Animals Mach.*, 2008, pp. 80–81.

[7] R. Niiyama, S. Nishikawa, and Y. Kuniyoshi, "Athlete robot with applied human muscle activation patterns for bipedal running," in *Proc. 10th IEEE RAS Int. Conf. Humanoid Robots*, 2010, pp. 498–503.

[8] K. Kawamura, R. A. Peters, D. M. Wilkes, W. A. Alford, and T. E. Rogers, "ISAC: Foundations in human-humanoid interaction," *IEEE Intell. Syst. Appl.*, vol. 15, no. 4, pp. 38–45, Jul./Aug. 2000.

[9] I. Boblan and A. Schulz, "A humanoid muscle robot torso with biologically inspired construction," in *Proc. ISR (41st Int. Symp. Robot.) ROBOTIK (6th German Conf. Robot.)*, 2010, pp. 1–6.

[10] S. Wongsiri and S. Laksanacharoen, "Design and construction of an artificial limb driven by artificial muscles for amputees," in *Proc. Int. Conf. Energy Environ.*, 2003, pp. 11–12.

[11] H. Kobayashi and K. Hiramatsu, "Development of muscle suit for upper limb," in *Proc. IEEE Int. Conf. Robot. Automat.*, vol. 3, 2004, pp. 2480–2485.

[12] J. He *et al.*, "Design of a robotic upper extremity repetitive therapy device," in *Proc. 9th Int. Conf. Rehabil. Robot.*, 2005, pp. 95–98.

[13] S. Balasubramanian *et al.*, "Rupert: An exoskeleton robot for assisting rehabilitation of arm functions," in *Proc. Virtual Rehabil.*, 2008, pp. 163–167.

[14] C. Vimieiro, B. G. do Nascimento, D. A. P. Nagem, and M. Pinotti, "Development of a hip orthosis using pneumatic artificial muscles," in *Proc. TMSi*, São Paulo, Spain, 2005, pp. 18–19.

[15] K. E. Gordon, G. S. Sawicki, and D. P. Ferris, "Mechanical performance of artificial pneumatic muscles to power an ankle-foot orthosis," *J. Biomech.*, vol. 39, no. 10, pp. 1832–1841, 2006.

[16] G. Brown, R. Haggard, R. Almassy, R. Benney, and S. Dellicker, "The affordable guided airdrop system (AGAS)," in *Proc. 15th Aerodynamic Decelerator Syst. Technol. Conf.*, 1999, Art. no. 1742.

[17] G. Olson, B. Woronowicz, and Y. Mengüç, "Characterization of a class of soft bending arms," in *Proc. 2nd IEEE Int. Conf. Soft Robot.*, 2019, pp. 462–469.

[18] M. Wehner *et al.*, "A lightweight soft exosuit for gait assistance," in *Proc. IEEE Int. Conf. Robot. Autom.*, 2013, pp. 3362–3369.

[19] B. Tondu and P. Lopez, "The McKibben muscle and its use in actuating robot-arms showing similarities with human arm behaviour," *Ind. Robot: An Int. J.*, vol. 24, no. 6, pp. 432–439, 1997, doi: 10.1108/01439919710192563.

[20] B. Tondu, "Modelling of the McKibben artificial muscle: A review," *J. Intell. Mater. Syst. Struct.*, vol. 23, no. 3, pp. 225–253, 2012.

[21] S. Koizumi, S. Kurumaya, H. Nabae, G. Endo, and K. Suzumori, "Braiding thin McKibben muscles to enhance their contracting abilities," *IEEE Robot. Automat. Lett.*, vol. 3, no. 4, pp. 3240–3246, Oct. 2018.

[22] S. Koizumi, S. Kurumaya, H. Nabae, G. Endo, and K. Suzumori, "Recurrent braiding of thin McKibben muscles to overcome their limitation of contraction," *Soft Robot.*, vol. 7, no. 2, pp. 251–258, 2020.

[23] D. Bruder, A. Sedal, R. Vasudevan, and C. D. Remy, "Force generation by parallel combinations of fiber-reinforced fluid-driven actuators," *IEEE Robot. Automat. Lett.*, vol. 3, no. 4, pp. 3999–4006, Oct. 2018.

[24] J. Bishop-Moser, G. Krishnan, and S. Kota, "Force and moment generation of fiber-reinforced pneumatic soft actuators," in *Proc. IEEE/RSJ Int. Conf. Intell. Robots Syst.*, 2013, pp. 4460–4465.